Acta Crystallographica Section B
Structural Science
ISSN 0108-7681

Chemical bonding and intermolecular interactions in energetic materials: 1,3,4-trinitro-7,8-diazapentalene

Yu-Sheng Chen,[a] Adam I. Stash[a,b] and A. Alan Pinkerton[a]*

[a]Department of Chemistry, University of Toledo, Toledo, OH 43606, USA, and [b]Karpov Institute of Physical Chemistry, Moscow, Russia

Correspondence e-mail: apinker@uoft02.utoledo.edu

Received 16 August 2006
Accepted 16 January 2007

The electron density and related properties of the red-colored energetic material 1,3,4-trinitro-7,8-diazapentalene (space group $Pca2_1$) have been determined from a low-temperature [90.0 (1) K] X-ray diffraction experiment. Intensity data were measured with a 2 K CCD Bruker diffractometer using Ag $K\alpha$ radiation. One detector setting, several φ settings, 0.15° ω scans and 96 s exposure time per frame gave R_{int} = 0.0188 for 31 952 (10 283 unique) reflections and $(\sin\theta/\lambda)_{max}$ = 1.15 Å^{-1}. The electron density was modeled using the Hansen–Coppens [(1978), *Acta Cryst.* A**34**, 909–921] multipole model and refined to R = 0.026 for 9455 unique observed reflections. The electron density, Laplacian and electrostatic potential distributions are reported and discussed. The properties of the bond (3,−1) critical points are analyzed. All results are indicative of multiple bonds in the five-membered rings. In addition, a significant number of weak intermolecular interactions (O···H, O···O, O···N, O···C) have also been characterized by the properties of their critical points. A comparison of experimental results with those obtained from theoretical calculations (periodic, *CRYSTAL*98; single molecule, *GAUSSIAN*98) is also reported.

1. Introduction

There has been a significant synthetic effort to design new energetic materials with low signature[1] and low shock sensitivity. Recent attention has focused on compounds based on aza derivatives of pentalene (1), in particular nitro derivatives of 2,5- and 7,8-diazapentalene (Butcher *et al.*, 2003*a*,*b*,*c*,*d*). In addition, empirical relationships between impact sensitivities and electrostatic potentials of energetic molecules calculated from theory have been proposed (Murray *et al.*, 1995; Rice & Hare, 2002). The earlier report found that the electrostatic potential on the molecular surface [surface with the electron density $\rho(r)$ = 0.001 a.u.] of all the shock-sensitive nitroheterocyclic molecules in their study contained maxima near the C—NO_2 bond. The later study extended the range of compounds to 54 and found some correlation between the charge separation in the molecules (as measured by the surface electrostatic potential) and impact sensitivity, however, the maxima were not in general over the C—NO_2 bonds. Thus, the pattern of surface electrostatic potential provides some guide in estimating impact sensitivity. However, we note that these computational studies were carried out on geometry-optimized molecules in the gas phase, whereas impact sensitivity is a property of the solid-state materials. Recently, it has been suggested (Bader, 2006) that the energy release owing to the rupture of intermolecular interactions

[1] Refers to the difficulty in detecting reaction products in the atmosphere, *e.g.* difficulty in detecting missile launches.

Table 1
Crystallographic data for (4).

Crystal data	
Chemical formula	$C_6H_3N_5O_6$
M_r	241.13
Cell setting, space group	Orthorhombic, $Pca2_1$
Temperature (K)	90 (1)
a, b, c (Å)	13.3229 (3), 7.0005 (1), 9.3471 (2)
V (Å^3)	871.78 (3)
Z	4
D_x (Mg m^{-3})	1.837
Radiation type	Ag $K\alpha$
μ (mm^{-1})	0.10
Crystal form, colour	Prism, red
Crystal size (mm)	0.30 × 0.25 × 0.21
Data collection	
Diffractometer	Smart CCD2000
Data collection method	ω
Absorption correction	None
No. of measured, independent and observed reflections	31 952, 10 283, 9455
Criterion for observed reflections	$I > 3\sigma$
R_{int}	0.019
θ_{max} (°)	40.1
Refinement	
Refinement on	F^2
$R[F^2 > 3\sigma(F^2)]$, $wR(F^2)$, S	0.026, 0.023, 1.44
No. of reflections	9455
No. of parameters	452
H-atom treatment	Refined independently
Weighting scheme	$w = 1/[\sigma^2(F^2)]$
$(\Delta/\sigma)_{max}$	<0.0001
$\Delta\rho_{max}$, $\Delta\rho_{min}$ (e Å^{-3})	0.16, −0.12
Extinction method	B–C type 1 Gaussian isotropic
Extinction coefficient	0.1188

Computer programs used: *SAINT* (Siemens, 1996), *SHELXTL* (Sheldrick, 1997), *XD* (Koritsanszky *et al.*, 2003).

may provide a pathway for the shock initiation of reaction. We have thus begun a study of the electron-density distribution, its topology and the derived electrostatic potential and energy-density distribution as well as intermolecular interaction energies for energetic materials in the solid state using data from X-ray diffraction experiments at very low temperature or from periodic theoretical calculations using experimental structural parameters.

In previous papers we presented the results for β-NTO (2) (Zhurova & Pinkerton, 2001; Zhurova *et al.*, 2004), PETN (3) (Zhurova *et al.*, 2006) and for the ammonium and biguanidinium salts of the dinitramide anion, ADN, (BIGH)(DN) and $(BIGH_2)(DN)_2$ (Zhurova, Martin *et al.*, 2002; Zhurova, Tsirelson *et al.*, 2002; Ritchie *et al.*, 2003). In the current paper we extend this work and present the results from a similar study on 1,3,4-trinitro-7,8-diazapentalene (4), whose structure was previously reported by Butcher *et al.* (2003*c*). The electron density has been refined using the Hansen–Coppens (1978) multipole model followed by analysis of the chemical bonding in (4) in terms of Bader's (1990) topological theory. Herein we report the electron density, Laplacian, electronic energy density and electrostatic potential distributions for (4) in the solid state determined from X-ray diffraction data and from theory. We discuss the characteristics of the intramolecular bond (3,−1) critical points, as well as the critical points observed for intermolecular interactions. In addition, comparison is made with results from a single molecule calculation in the gas phase at the experimental geometry.

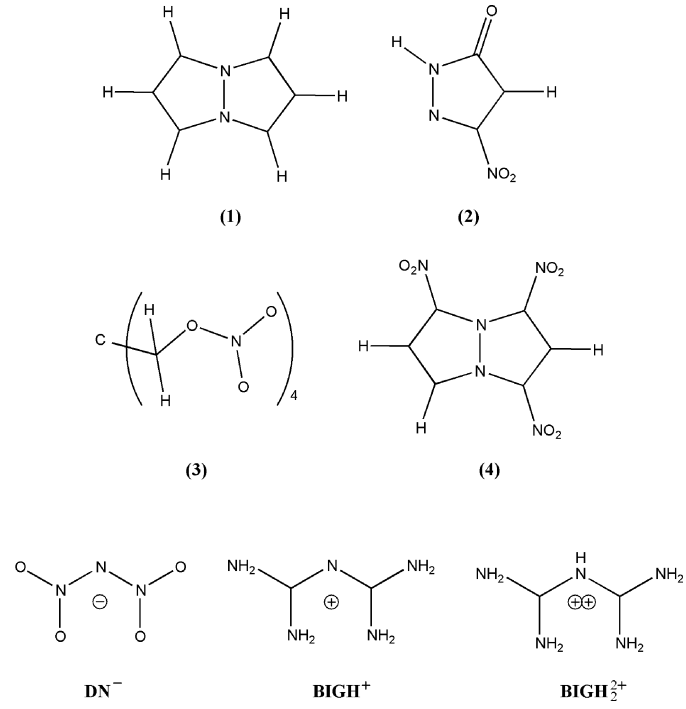

2. Experimental

A red single crystal of (4) grown from acetonitrile solution was mounted on a 0.1 mm capillary with epoxy resin and slowly cooled down to 90 K with an Oxford Cryostream. A preliminary X-ray diffraction experiment was performed with a Bruker platform diffractometer with a 2 K CCD detector using Ag $K\alpha$ radiation and the structure was redetermined to establish the protocol for charge-density data collection.

For the charge density data, 3300 frames (0.15° ω scans) were collected at φ values of 45, 135 and 225°, followed by 200 additional frames at 45° in order to monitor intensity decay. There is no evidence to indicate any intensity decay during the experiment. The distance between the detector and the crystal was 2.7 cm at a swing angle of −51.5°. The exposure time of 96 s allowed the use of the full dynamic range of the 2 K CCD detector.

The frames were integrated using the program *SAINT* (Siemens, 1996). A correction for oblique incidence (Wu *et al.*, 2002) was applied and the data were then sorted and merged with the program *SORTAV* (Blessing, 1987, 1989). A total of 31 952 reflections were integrated ($\sin\theta/\lambda < 1.15$ Å^{-1}), of which 10 283 with $I \geq 1\sigma(I)$ were unique ($R_{int} = 0.0188$). The final unit-cell parameters were obtained from the reflection XYZ centroids for the whole data set. The crystallographic data are summarized in Table 1.

Table 2
Selected bond lengths (Å) and angles (°) for (4).

O11—N1	1.2333 (6)	N7—N8	1.3617 (4)
O12—N1	1.2301 (6)	N7—C1	1.3832 (5)
O31—N3	1.2324 (7)	N7—C6	1.3696 (5)
O32—N3	1.2324 (7)	N8—C3	1.3818 (5)
O41—N4	1.2308 (6)	N8—C4	1.3640 (5)
O42—N4	1.2329 (6)	C1—C2	1.3827 (5)
N1—C1	1.4040 (5)	C2—C3	1.3879 (5)
N3—C3	1.4064 (5)	C4—C5	1.3997 (5)
N4—C4	1.4080 (5)	C5—C6	1.3804 (6)
O11—N1—O12	124.98 (4)	C3—N8—C4	144.26 (3)
O11—N1—C1	117.79 (4)	N1—C1—N7	121.40 (4)
O12—N1—C1	117.23 (4)	N1—C1—C2	129.22 (4)
O31—N3—O32	124.49 (4)	N7—C1—C2	109.31 (3)
O31—N3—C3	116.91 (5)	C1—C2—C3	106.06 (3)
O32—N3—C3	118.56 (4)	N3—C3—N8	122.48 (4)
O41—N4—O42	124.78 (5)	N3—C3—C2	126.33 (4)
O41—N4—C4	118.06 (4)	N8—C3—C2	108.68 (3)
O42—N4—C4	117.07 (4)	N4—C4—N8	121.43 (3)
N8—N7—C1	107.49 (3)	N4—C4—C5	127.63 (4)
N8—N7—C6	109.92 (3)	N8—C4—C5	108.37 (3)
C1—N7—C6	142.57 (3)	C4—C5—C6	107.12 (3)
N7—N8—C3	108.34 (3)	N7—C6—C5	107.16 (3)
N7—N8—C4	107.40 (3)		

3. Refinements and results

The crystal structure was redetermined and a preliminary refinement of the positional and atomic displacement parameters was carried out with the *SHELXTL* program suite (Sheldrick, 1997). In subsequent refinements, the Hansen–Coppens (1978) multipole model, as implemented in the *XD* program (Koritsanszky *et al.*, 2003) was used. In this model the electron density is approximated as the sum of pseudo-atomic electron densities, the optimized parameters being a scale factor, the atomic valence-shell contraction–expansion parameters κ' and κ'', and the multipole populations P_v and P_{lm}, in addition to the positional and displacement parameters.

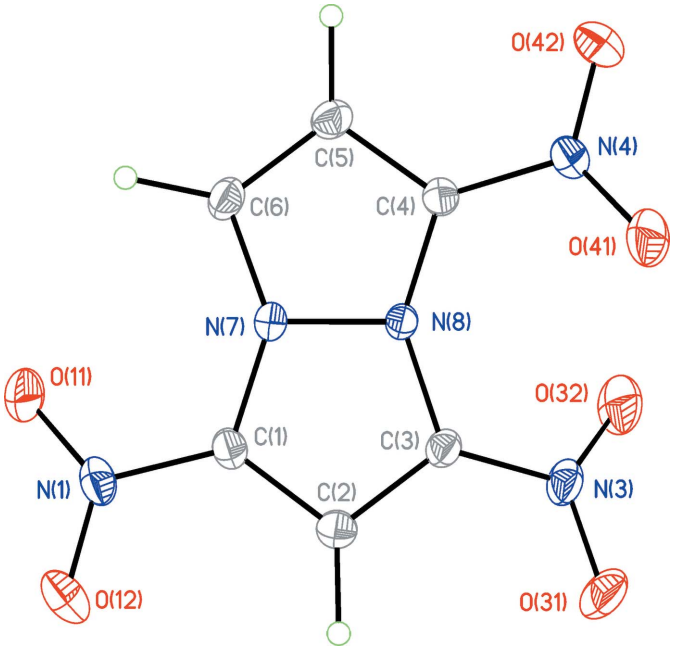

Figure 1
Molecule (4), showing 75% probability displacement ellipsoids.

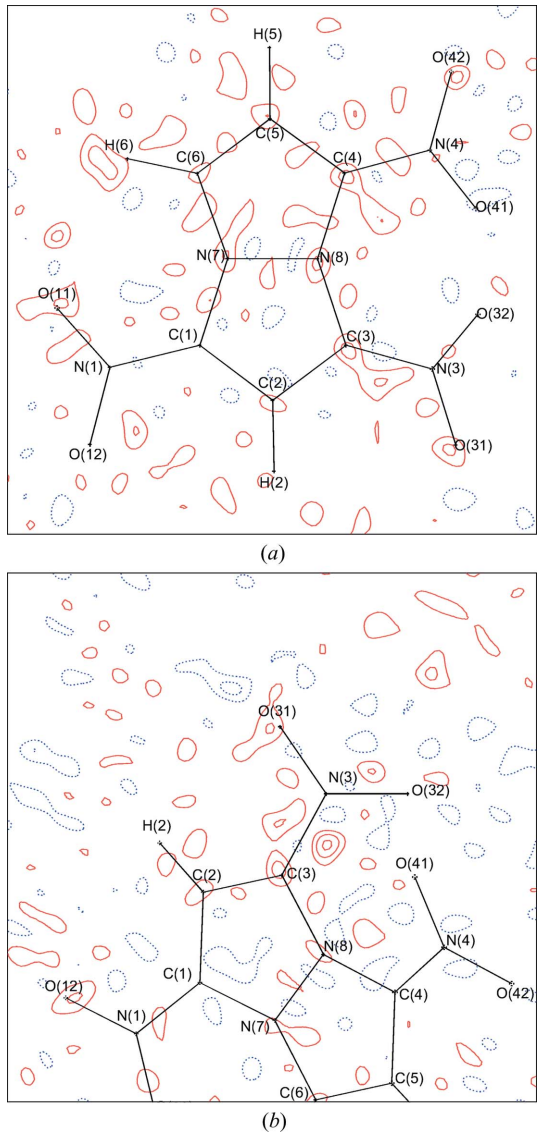

Figure 2
Difference electron density map ($\delta\rho_{\rm resid}$) (*a*) in the plane of the diazapentalene rings, (*b*) in the plane of one (N3) nitro group. Here and in Fig. 3 positive contours are solid (red) lines, negative are dotted (blue). The contour interval is 0.05 e Å^{-3}.

Since the space group is non-centrosymmetric, a very conservative approach was adopted for the refinement. The refinement was carried out on $|F^2|$ using only reflections with $I > 3\sigma(I)$. In a first step, the positional and anisotropic displacement parameters for the non-H atoms were refined using high-angle data ($\sin\theta/\lambda > 0.7$ Å^{-1}), keeping the scale factor fixed to the value from a prior spherical atom refinement using the whole data set. Next the positional and isotropic displacement parameters for the H atoms were refined using low-angle data ($\sin\theta/\lambda < 0.7$ Å^{-1}). At this point the H atoms were moved along the bond vector to appropriate neutron positions (Allen *et al.*, 1987; C—H, 1.08 Å). The parameters obtained at this point were used as the starting

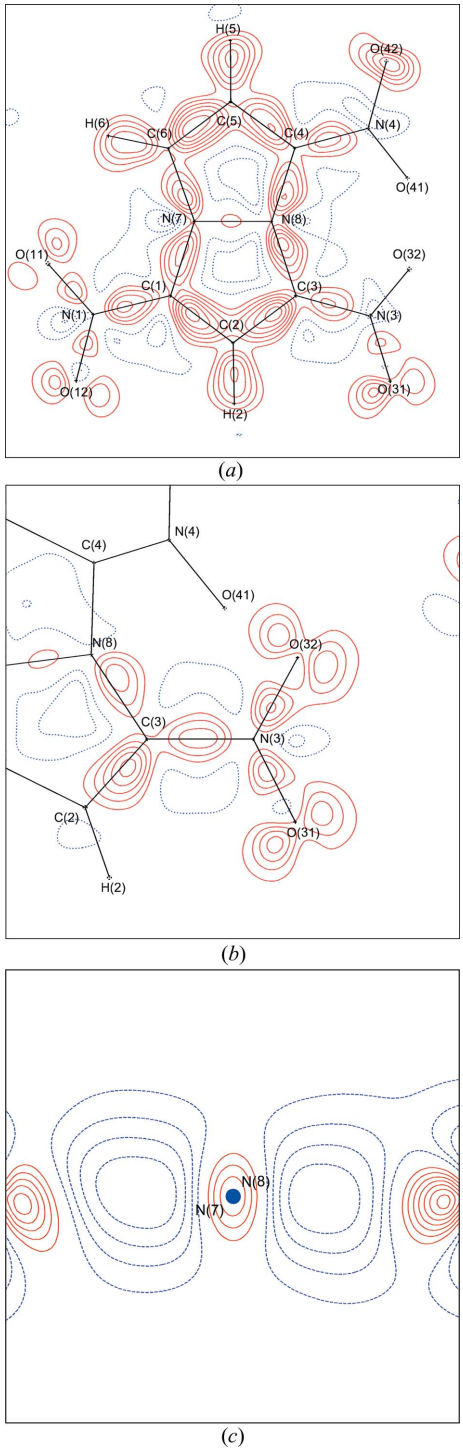

Figure 3
Deformation density maps ($\delta\rho_{\rm mult}$): (*a*) in the plane of the diazapentalene rings, (*b*) in the plane of one (N3) nitro group, (*c*) perpendicular section through N7—N8. The contour interval is 0.1 e Å^{-3} for *a*, *b* and 0.05 e Å^{-3} for *c*.

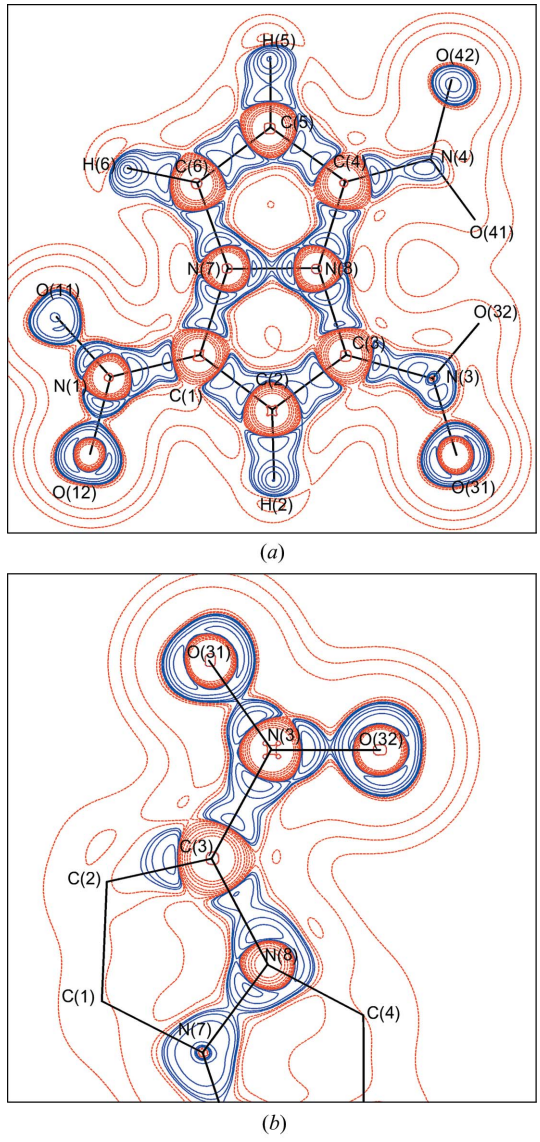

Figure 4
The Laplacian of the electron density (*a*) in the plane of the diazapentalene rings, (*b*) in the plane of one (N3) nitro group. Contour intervals are $\pm2\times10^n$, $\pm4\times10^n$, $\pm8\times10^n$ (n = 0, 1, 2) e Å^{-5}. Solid line (blue) – negative Laplacian, dotted line (red) – positive Laplacian.

model for a kappa refinement (Coppens *et al.*, 1979) using the whole data set with $I > 3\sigma(I)$, in which κ' and the monopole populations were varied within the constraints O11 = O12 = O31 = O32 = O41 = O42, N1 = N3 = N4, N7 = N8, C1 = C3 = C4, C2 = C5 = C6, H2 = H5 = H6. The charge neutrality constraint was applied throughout. Using the same chemical constraints plus mirror symmetry (approximately the molecular plane) for each atom, each set of multipoles up to the octupole level (one dipole and one quadrupole for H atoms at this point) were refined in turn, the process being recycled until convergence.[2] All of the multipoles were then refined together, followed by the positional and displacement parameters with fixed multipole populations, followed by the scale factor alone. At this point, κ' and the monopole populations were refined again and the whole process was repeated. This same cycling procedure was repeated with the gradual release of the constraints. First the chemical constraints on the

[2] Supplementary data, including the local coordinate systems used for all pseudo atoms, for this paper are available from the IUCr electronic archives (Reference: BS5038). Services for accessing these data are described at the back of the journal.

Table 3
Properties of critical points in (4).

(*a*) Bond critical points.

First rows – multipole model from experimental structure factors; second rows – multipole model from theoretical structure factors (*CRYSTAL*98); third rows – direct theoretical calculation by *GAUSSIAN*98. R_{ij} is the interatomic distance, d_1 and d_2 are the distances from the critical point to atoms 1 and 2, ρ is the electron density, $\nabla^2\rho$ is the Laplacian, λ_1, λ_2, λ_3 are principle curvatures, ε is bond ellipticity and $n_{\rm topo}$ is topological bond order.

Bond	R_{ij} (Å)	d_1 (Å)	d_2 (Å)	ρ (e Å^{-3})	$\nabla^2\rho$ (e Å^{-5})	λ_1 (e Å^{-5})	λ_2 (e Å^{-5})	λ_3 (e Å^{-5})	ε	$n_{\rm topo}$
O11—N1	1.233	0.641	0.592	3.27	−11.6	−31.82	−28.09	48.36	0.13	1.83
	1.233	0.633	0.600	3.21	−8.3	−27.74	−26.69	46.15	0.04	1.84
	1.233	0.642	0.591	3.30	−23.5	−31.04	−27.98	35.55	0.11	1.60
O12—N1	1.230	0.652	0.578	3.26	−10.0	−31.53	−27.08	48.65	0.16	1.85
	1.230	0.633	0.597	3.23	−8.7	−28.05	−26.86	46.17	0.05	1.85
	1.230	0.639	0.591	3.33	−23.5	−31.16	−28.12	35.74	0.11	1.62
O31—N3	1.232	0.634	0.599	3.30	−8.7	−31.07	−27.57	49.94	0.13	1.91
	1.232	0.630	0.603	3.25	−9.6	−28.08	−27.26	45.70	0.03	1.84
	1.232	0.640	0.592	3.31	−23.2	−30.99	−27.93	35.74	0.11	1.61
O32—N3	1.232	0.638	0.595	3.37	−9.9	−31.94	−28.70	50.76	0.11	1.94
	1.232	0.631	0.602	3.26	−10.0	−28.07	−27.67	45.73	0.01	1.84
	1.232	0.642	0.590	3.31	−23.3	−31.04	−27.88	35.62	0.11	1.61
O41—N4	1.231	0.632	0.599	3.29	−9.3	−32.23	−26.23	49.20	0.23	1.89
	1.231	0.630	0.601	3.23	−8.7	−27.74	−26.80	45.84	0.04	1.84
	1.231	0.641	0.589	3.32	−23.6	−31.21	−28.05	35.62	0.11	1.61
O42—N4	1.233	0.610	0.624	3.22	−6.7	−28.78	−26.54	48.60	0.08	1.88
	1.233	0.630	0.603	3.20	−8.3	−27.59	−26.31	45.57	0.05	1.83
	1.233	0.640	0.593	3.31	−23.1	−30.92	−27.91	35.74	0.11	1.61
N1—C1	1.404	0.821	0.583	2.06	−18.3	−18.92	−13.54	14.20	0.40	0.92
	1.404	0.820	0.585	2.02	−15.3	−16.33	−13.04	14.05	0.25	0.97
	1.404	0.870	0.534	2.04	−21.1	−16.74	−12.55	8.20	0.33	0.94
N3—C3	1.406	0.798	0.608	2.03	−15.9	−18.25	−13.22	15.53	0.38	0.94
	1.406	0.820	0.587	1.98	−14.8	−16.00	−12.75	14.00	0.26	0.93
	1.407	0.865	0.542	2.03	−21.3	−16.69	−12.87	8.22	0.30	0.93
N4—C4	1.408	0.797	0.611	2.11	−16.9	−19.38	−13.71	16.21	0.41	0.99
	1.408	0.816	0.592	1.99	−15.0	−16.23	−13.00	14.25	0.25	0.93
	1.408	0.866	0.543	2.03	−21.3	−16.61	−12.88	8.21	0.29	0.92
N7—N8	1.362	0.683	0.679	2.28	−4.3	−19.91	−16.34	31.97	0.22	1.39
	1.362	0.682	0.679	2.30	−4.2	−19.42	−16.67	31.88	0.17	1.44
	1.362	0.680	0.682	2.46	−16.8	−22.10	−17.89	23.20	0.24	1.23
N7—C1	1.383	0.787	0.597	2.14	−17.4	−18.50	−14.65	15.79	0.26	1.03
	1.383	0.817	0.567	2.01	−13.9	−15.48	−12.66	14.22	0.22	0.99
	1.384	0.901	0.482	1.96	−12.8	−14.25	−10.17	11.62	0.40	1.02
N7—C6	1.370	0.832	0.538	2.04	−17.1	−15.67	−13.09	11.62	0.20	1.00
	1.370	0.834	0.536	2.00	−14.8	−14.25	−12.79	12.23	0.11	0.99
	1.370	0.904	0.466	1.95	−7.7	−12.80	−10.87	15.99	0.18	1.07
N8—C3	1.382	0.831	0.554	2.04	−17.9	−17.68	−12.99	12.82	0.36	0.95
	1.382	0.813	0.571	1.99	−13.9	−15.46	−12.77	14.27	0.21	0.97
	1.382	0.903	0.479	1.95	−11.7	−13.90	−10.04	12.29	0.38	1.02
N8—C4	1.364	0.807	0.558	2.17	−19.3	−18.88	−14.23	13.80	0.33	1.05
	1.364	0.813	0.552	2.08	−15.6	−16.35	−12.92	13.66	0.27	1.04
	1.365	0.895	0.470	2.02	−10.9	−14.70	−10.52	14.37	0.40	1.09
C1—C2	1.383	0.738	0.645	2.17	−18.6	−17.01	−13.46	11.84	0.26	1.39
	1.383	0.706	0.677	2.12	−15.8	−15.70	−13.12	13.05	0.20	1.48
	1.383	0.722	0.661	2.12	−20.9	−15.95	−12.42	7.48	0.28	1.38
C2—C3	1.388	0.663	0.725	2.19	−19.0	−17.19	−13.98	12.15	0.23	1.35
	1.388	0.683	0.705	2.04	−14.9	−15.06	−12.61	12.81	0.19	1.40
	1.388	0.665	0.723	2.10	−20.6	−15.86	−12.30	7.58	0.29	1.38
C4—C5	1.400	0.719	0.682	2.04	−16.2	−15.96	−12.38	12.15	0.29	1.31
	1.400	0.721	0.679	1.98	−13.6	−14.48	−12.04	12.87	0.20	1.37
	1.400	0.738	0.662	2.05	−19.8	−15.31	−12.12	7.65	0.26	1.33
C5—C6	1.380	0.677	0.703	2.29	−19.9	−18.09	−13.99	12.19	0.29	1.51
	1.380	0.674	0.707	2.12	−16.3	−15.37	−13.18	12.25	0.17	1.48
	1.380	0.672	0.709	2.14	−21.2	−16.17	−12.56	7.55	0.29	1.39
C2—H2	1.080	0.706	0.375	1.91	−18.2	−18.98	−17.52	18.31	0.08	1.01
	1.080	0.712	0.368	1.84	−17.1	−17.73	−16.97	17.63	0.05	0.99
	1.064	0.715	0.349	1.92	−24.5	−19.34	−19.05	13.92	0.02	0.86
C5—H5	1.080	0.668	0.412	1.99	−20.7	−18.99	−18.13	16.46	0.05	1.04
	1.080	0.715	0.365	1.87	−18.1	−18.06	−17.67	17.59	0.02	0.98
	1.064	0.709	0.356	1.92	−24.2	−19.05	−18.68	13.56	0.02	0.88
C6—H6	1.080	0.690	0.391	1.93	−18.8	−19.05	−17.47	17.69	0.09	1.02
	1.080	0.717	0.364	1.88	−18.5	−18.61	−17.43	17.58	0.07	0.98
	1.064	0.715	0.348	1.94	−24.6	−19.72	−18.91	14.00	0.04	0.87

Table 3 (continued)

Bond	R_{ij} (Å)	d_1 (Å)	d_2 (Å)	ρ (e Å^{-3})	$\nabla^2\rho$ (e Å^{-5})	λ_1 (e Å^{-5})	λ_2 (e Å^{-5})	λ_3 (e Å^{-5})	ε	n_{topo}
O11···H6	2.515	1.400	1.140	0.08	1.2	−0.26	−0.19	1.64	0.35	–
	2.515	1.400	1.154	0.07	1.1	−0.23	−0.14	1.43	0.64	–
	2.596	1.461	1.135	0.08	1.1	−0.24	−0.10	1.40	1.33	–
O32···O41	2.551	1.284	1.267	0.13	2.2	−0.47	−0.42	3.12	0.13	–
	2.551	1.277	1.274	0.12	2.1	−0.44	−0.40	2.96	0.12	–
	2.553	1.274	1.279	0.13	2.0	−0.45	−0.42	2.82	0.06	–

(*b*) Intermolecular critical points.

First rows: multipole model from experimental structure factors; second rows: multipole model from theoretical structure factors (*CRYSTALS*98). R_{ij} is the interatomic distance, d_1 and d_2 are the distances from the critical point to atoms 1 and 2, ρ is the electron density, $\nabla^2\rho$ is the Laplacian, g is the kinetic energy density, v is the potential energy density, h is the total electronic energy density, D_e is the estimated dissociation energy.

Bond	R_{ij} (Å)	d_1 (Å)	d_2 (Å)	ρ (e Å^{-3})	$\nabla^2\rho$ (e Å^{-5})	g (a.u.)	v (a.u.)	h (a.u.)	D_e (kJ mol^{-1})
O11···H5^{i}	2.817	1.659	1.221	0.02	0.3	0.0023	−0.0014	0.0009	1.8
	2.817	1.608	1.220	0.02	0.4	0.0027	−0.0017	0.0010	2.2
O32···H5^{ii}	2.453	1.479	1.031	0.04	0.7	0.0056	−0.0038	0.0019	5.0
	2.453	1.421	1.044	0.06	0.8	0.0068	−0.0049	0.0019	6.4
O42···H2^{iii}	2.301	1.433	0.887	0.05	1.0	0.0079	−0.0052	0.0027	6.8
	2.301	1.376	0.932	0.07	1.1	0.0090	−0.0067	0.0023	8.8
O42···H6^{iv}	2.414	1.454	0.984	0.04	0.7	0.0055	−0.0037	0.0018	4.9
	2.414	1.459	0.958	0.05	0.8	0.0063	−0.0044	0.0019	5.8
O11···O42^{i}	2.876	1.432	1.445	0.05	0.9	0.0073	−0.0050	0.0023	6.6
	2.876	1.436	1.440	0.05	0.9	0.0067	−0.0045	0.0022	5.9
O11···O31^{v}	2.995	1.509	1.501	0.05	0.8	0.0063	−0.0043	0.0020	5.6
	2.995	1.509	1.500	0.04	0.8	0.0060	−0.0040	0.0020	5.2
O31···N1^{vi}	2.923	1.425	1.546	0.06	1.0	0.0084	−0.0060	0.0024	7.9
	2.923	1.423	1.512	0.06	0.9	0.0075	−0.0054	0.0021	7.1
O41···N8^{vi}	2.789	1.371	1.420	0.08	1.3	0.0106	−0.0080	0.0026	10.5
	2.789	1.344	1.445	0.09	1.3	0.0110	−0.0085	0.0025	11.1
O12···C4^{vii}	3.028	1.446	1.622	0.06	0.9	0.0072	−0.0053	0.0019	7.0
	3.028	1.440	1.618	0.06	0.9	0.0069	−0.0050	0.0019	6.6
O12···C5^{viii}	3.195	1.551	1.655	0.04	0.5	0.0042	−0.0028	0.0014	3.7
	3.195	1.544	1.671	0.03	0.5	0.0041	−0.0027	0.0014	3.5
O31···C6^{ix}	3.003	1.460	1.578	0.05	0.8	0.0062	−0.0043	0.0019	5.6
	3.003	1.450	1.569	0.05	0.8	0.0062	−0.0043	0.0019	5.6

Symmetry codes: (i) $-x, 1-y, -\frac{1}{2}+z$; (ii) $\frac{1}{2}+x, 1-y, z$; (iii) $\frac{1}{2}-x, 1+y, \frac{1}{2}+z$; (iv) $-x, 1-y, \frac{1}{2}+z$; (v) $-\frac{1}{2}+x, -y, z$; (vi) $\frac{1}{2}-x, y, \frac{1}{2}+z$; (vii) $-x, -y, -\frac{1}{2}+z$; (viii) $x, -1+y, z$; (ix) $\frac{1}{2}+x, -y, z$.

multipole populations were removed from the O atoms. After convergence, the nitrogen constraints were removed and in subsequent cycles, the carbon and hydrogen constraints. At this point, the κ'' were refined with the same constraints as for κ' and then fixed. The final constraint, the imposed mirror symmetry, was then removed[3] and the cycling procedure repeated. This slow approach to convergence was found to be necessary, as the refinement became unstable in the early stages if too many variables were introduced at the same time. At convergence, $R = 0.026$ for 9455 reflections with $I > 3\sigma(I)$.

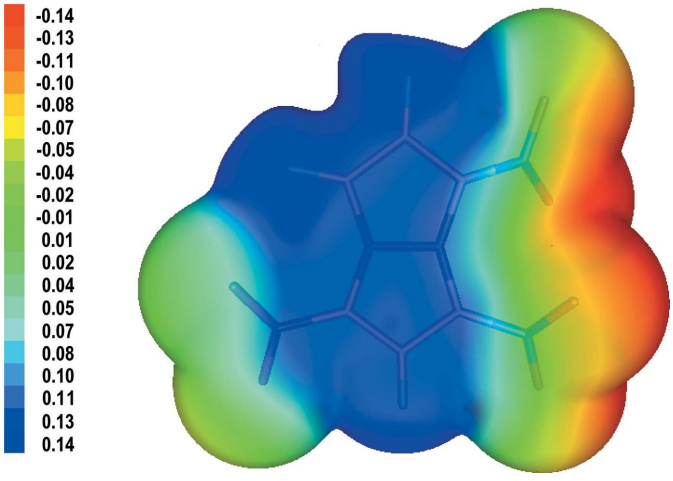

Figure 5
Electrostatic potential of the isolated molecule projected onto the molecular surface [$\rho(r) = 0.001$ a.u.]. Units are e Å^{-1}.

The rigid-bond test (Hirshfeld, 1976) showed that the differences of mean-square displacement amplitudes along the interatomic vectors were less than 6×10^{-4} Å^2. The largest least-squares correlation coefficient observed was 0.60. The atomic displacement ellipsoids (75% probability) are shown in Fig. 1 and the interatomic distances and angles are included in Table 2. The multipole, kappa, positional and displacement parameters have been deposited.

The residual electron density in the plane of the molecule (the difference between experimental and calculated multipole electron densities: $\delta\rho_{res} = \rho_{exp} - \rho_{mult}$) calculated with the low-angle reflections ($\sin\theta/\lambda < 1.0$ Å^{-1}) is presented in Fig. 2(*a*), and the static model multipole deformation electron

[3] Note that this implies that all three dipoles were refined for the H atoms, but still only one quadrupole.

density (the difference between calculated multipole and spherical static electron densities: $\delta\rho_{mult} = \rho_{mult} - \rho_{sph}$) in Fig. 3(*a*) in the plane of the molecule. Similar maps in the plane of one of the nitro groups are reported in Figs. 2(*b*) and 3(*b*). The topological analysis of the total electron density was performed with the program *WinXPRO* (Stash & Tsirelson, 2002, 2005). The same program was used to obtain the atomic charges from integration over the atomic basins. Using the static multipole model of the electron density, the Laplacian and electrostatic potential distributions (Su & Coppens, 1992; Tsirelson & Ozerov, 1996; Tsirelson *et al.*, 2000) were also calculated. The Laplacian is reported in Fig. 4(*a*) in the molecular plane, and in Fig. 4(*b*) for one nitro group. The electrostatic potential projected onto the molecular surface [$\rho(r)$ = 0.001 a.u.] is shown in Fig. 5. The properties of the bonding (3,−1) critical points which characterize the covalent bonding in (4) are given in Table 3(*a*). To compare with the experimental result, a theoretical calculation (DFT/B3LYP, 6-311G** basis set with the constrained experimental geometry) was also performed using the program *CRYSTAL*98 (Saunders *et al.*, 1998), for the crystal and for a single molecule in the gas phase with the same geometry (pseudo-isolated molecule) using the same basis set with *GAUSSIAN*98 (Frisch *et al.*, 1998). An additional refinement of the multipole model based on the theoretically calculated structure factors was also carried out followed by a topological analysis of the electron density. The resulting properties of the intramolecular bond-critical points are reported and compared in Table 3(*a*). A number of intermolecular C—H···O interactions in crystals of (4) were reported by Butcher *et al.* (2003*c*), hence we have searched the intermolecular regions for critical points in the electron density in order to characterize all the intermolecular interactions. The results are reported in Table 3(*b*), and an example showing two O···O interactions is shown in Fig. 6.

4. Discussion

The structural parameters of (4) agree closely with those previously reported (Butcher *et al.*, 2003*c*) and the salient features may be summarized as follows. The molecular skeleton (excluding the nitro groups) is essentially planar, the fold around the N7—N8 bond being only 2.3°. Steric interactions twist the planar nitro groups out of the molecular plane (N1, O11, O12, 12.2°; N3, O31, O32, 27.9°; N4, O41, O42, 22.1°, the dihedral angles being defined by the plane of the CNO_2 unit and that of the bound C atom), and introduce some pyramidalization of C3 (0.127 Å), and C4 (0.129 Å) (distances out of the plane taken through neighboring atoms). The same interaction may be responsible for pushing the H2 atom out of the plane of the neighboring carbon atoms by 0.122 Å, however, there is also a contribution from hydrogen bonding (see below). Examination of the bond lengths (Table 2) already suggests multiple bonding in the pentalene rings (albeit with some asymmetry in the monosubstituted ring), as well as to the nitro groups despite the twist angles.

Fig. 2 presents the residual map after the multipole refinement in the diazapentalene plane and in the plane of one of the nitro groups (the other nitro groups being essentially identical). The largest residual in the unit cell is a maximum of 0.16 e Å^{-3}, however, there are no peaks greater than ±0.05 e Å^{-3} on the interatomic bonds. Fig. 3 presents deformation electron density ($\delta\rho_{mult}$) maps, (*a*) in the molecular plane and (*b*) in the plane of one nitro group. Every expected covalent bond is represented by well defined $\delta\rho_{mult}$ peaks. Polarization of the C—N bonds in the ring structure is clearly seen, whereas the other ring bonds appear to be non-polar. The N7—N8 bond is of particular interest. The $\delta\rho_{mult}$ peak on the N7—N8 line is only *ca* 0.1 e Å^{-3} compared with other bonds in the ring of *ca* 0.4–0.6 e Å^{-3}, and it is also quite diffuse in the plane perpendicular to the bond (Fig. 3*c*). However, the interatomic distance is still quite short at 1.3617 (4) Å. This situation is almost identical to that observed for the five-membered ring in β-NTO (Zhurova & Pinkerton, 2001), however, see below for a discussion of the properties of the (3,−1) critical point in the total electron density.

The NO_2 groups are quite symmetrical with two well developed oxygen lone-pair regions essentially in the plane of the nitro groups, the O Lp vectors being essentially perpendicular to the N—O bonds as has been previously observed (Volkov *et al.*, 2000; Zhurova & Pinkerton, 2001; Zhurova *et al.*, 2002).

The Laplacian of the electron density in the molecular plane is shown in Fig. 4(*a*) and that in the plane of one of the nitro groups in Fig. 4(*b*). The blue contours show the negative values of the Laplacian, *i.e.* they represent the accumulation of electron density in the crystal. For (4), as anticipated, this accumulation is mostly around the atoms and along the chemical bonds. For the O atoms, the electron density concentrates mainly in the non-bonding directions, again emphasizing the lone-pair regions. The accumulation of elec-

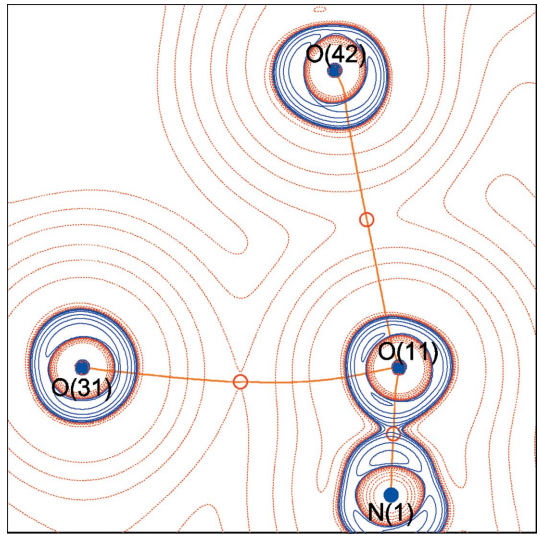

Figure 6
Laplacian of the total electron density in the plane of the atoms O11—O31—O42. Contour intervals are $\pm2.10^n$, $\pm4.10^n$, $\pm8.10^n$ (n = −1, 0, 1, 2) e Å^{-5}. Blue line – negative Laplacian, red line – positive Laplacian. Bond paths are shown in orange and the (3,−1) critical points as red circles.

Table 4
Integrated properties of atoms in (4).

Exp. – multipole model from experimental structure factors; theor. – multipole model from theoretical structure factors (*CRYSTAL*98). Ω = atomic volume delimited by zero flux surface; q = atomic charge from integration of the electron density over the atomic basin minus Z; H = total electronic energy from integration over the atomic basin; V_{cell} = 871.776 Å^3; H = −954.947 a.u. (*GAUSSIAN*98); Q_{mol} = 122 e.

	Ω (Å^3)		q (e)		H (a.u.)		$\frac{1}{4}\nabla^2\rho$ ($\times 10^{-4}$ a.u.)	
Atom	Exp.	Theor.	Exp.	Theor.	Exp.	Theor.	Exp.	Theor
O11	15.868	15.466	-0.438	−0.376	−74.890	−75.093	−4.0	−0.8
O12	16.410	16.025	−0.434	−0.399	−74.856	−75.165	−5.5	−4.1
O31	16.072	15.711	−0.483	−0.367	−75.036	−75.072	−0.9	−4.4
O32	16.778	16.228	−0.506	−0.392	−75.134	−75.167	−5.0	−0.7
O41	15.506	15.184	−0.446	−0.386	−74.926	−75.130	−6.2	−13.9
O42	17.734	17.118	−0.373	−0.371	−74.729	−75.074	−3.2	−3.9
N1	7.003	6.837	0.433	0.359	−54.140	−54.473	−3.2	5.1
N3	7.503	7.522	0.347	0.356	−54.402	−54.479	2.8	3.2
N4	8.492	8.454	0.388	0.362	−54.320	−54.457	−6.4	4.9
N7	9.572	9.549	−0.501	−0.572	−55.155	−55.400	−8.7	−5.7
N8	8.777	8.796	−0.515	−0.527	−55.241	−55.321	−5.9	−8.0
C1	8.174	8.512	0.557	0.476	−38.061	−38.116	4.1	−5.7
C2	11.033	11.105	0.160	0.069	−38.337	−38.453	0.8	−5.2
C3	8.541	8.633	0.520	0.554	−38.089	−37.960	5.7	8.4
C4	8.548	8.911	0.586	0.547	−38.013	−37.986	6.2	7.5
C5	11.115	11.377	0.107	0.062	−38.418	−38.428	6.3	−6.3
C6	11.320	11.630	0.360	0.301	−38.160	−38.177	6.2	−2.7
H2	6.269	7.024	0.138	0.098	−0.559	−0.549	−2.5	−0.6
H5	6.322	6.773	0.048	0.093	−0.651	−0.554	−4.2	−0.1
H6	6.763	6.876	0.055	0.115	−0.623	−0.544	−1.9	−-0.9
Total	217.801	217.729	0.003	0.003	−953.739	−955.597		

tron density in the N7—N8 bond contrasts with the inadequate picture obtained above from the deformation density.

The electrostatic potential distribution was also calculated using the refined multipole model. Fig. 5 shows the electrostatic potential on the molecular surface (*gOpenMol*, 2005 http://www.csc.fi/gopenmol/; Laaksonen, 1992; Bergman *et al.*, 1997) for the isolated molecule taken from the crystal. Using the rational of Rice & Hare (2002), the charge separation represented by the form of the electrostatic potential implies that (4) should be moderately shock sensitive. To our knowledge, the shock sensitivity of (4) (h_{50}) has not been reported. The expected negative regions around the nitro groups are observed. The potential is particularly negative in the region between the two neighboring nitro groups, indicating a cooperative effect and introducing asymmetry into the potential. The potential around the third nitro group is significantly less negative. These negative regions represent the sites of potential electrophilic attack.

A more quantitative measure of the bonding interactions may be obtained from the topological analysis of the total electron density. Table 3(*a*) lists the properties of all the (3,−1) critical points found in the molecule: for each bond the first line lists the experimental results, the second line contains the results after the multipole refinement based on theoretically calculated structure factors (*CRYSTAL*98) and the third line reports the values obtained for a single molecule in the gas phase (*GAUSSIAN*98). As there is satisfactory agreement in the trend in the properties at the CP from theory and experiment, the following discussion is based on the experimentally determined values. The only significant differences are between values of the Laplacian obtained from the multipole model and theory, as has been previously discussed (Bianchi *et al.*, 1996; Spackman *et al.*, 1999; Flaig *et al.*, 2002; Volkov *et al.*, 2004; Coppens & Volkov, 2004; Zhurova *et al.*, 2004; Henn *et al.*, 2004; Tsirelson *et al.*, 2006).

The value of the electron density at the critical point is significant for all bonds, indicating strong covalent bonds. However, it is significantly greater for the nitro-group N—O bonds than for all of the N—N, C—N and C—C bonds in the rest of the molecule (3.22–3.37 *versus* 2.03–2.28 e Å^{-3}). From the position of the critical points, significant polarization of the N—C bonds may be concluded, however, the N—O bonds are less polarized and, not surprisingly, the N—N and C—C bonds are non-polar. As was observed for β-NTO, the electron density at the critical point of the N7—N8 bond (2.28 e Å^{-3}) is similar to the other bonds in the diazapentalene rings, however, it has the least negative Laplacian value (−4.28 *versus* −20.21 to −15.06 e Å^{-5}). This is due to the high positive value for the λ_3 eigenvalue (31.97 e Å^{-5}), indicating that the charge depletion in the bond direction is approximately double that of the other ring bonds. Although there are few examples in the literature, this feature of the N—N bond has been previously noted. There are two N—N bonds in trimethylammonionitramidate, $(CH_3)_3N1^+—N2^-—N3O_2$, N1—N2 having $\nabla^2\rho$ = −2.52 e Å^{-5}, whereas that of N2—N3 is more 'normal' at −30.6 e Å^{-5} (Smith *et al.*, 1997). One might attribute this 'normal value' to the presence of the O atoms, however, four values obtained for the N—N bonds in the

dinitramide anion, $(O_2N-N-NO_2)^-$, range from −4.24 to −8.22 e Å^{-5} (Zhurova *et al.*, 2002). The final example is of a tetrazole ring in the molecule $C_{30}H_{39}N_6O_3S$, where $\nabla^2\rho$ for the three N—N bonds range from −8 to – 13 e Å^{-5} (Destro *et al.*, 2005).

The ellipticities are generally higher (av. 0.27) for the ring bonds than for the N—O bonds (av. 0.14). These values are similar to those observed in β-NTO and indicate a significant π component to all the bonds in the molecular skeleton. Indeed, the similarities of the properties of the N—N, C—N and C—C bonds in terms of the electron density and ellipticity suggest total conjugation. However, when calculating topological bond orders from the electron density values (ρ) and the principle electron-density curvatures (λ_1, λ_2, λ_3) at the bond critical points (Table 3*a*) as $n_{\rm topo} = a + b(\lambda_1 + \lambda_2) + c\lambda_3 + d\rho_{\rm CP}$

a	*b*	*c*	*d*	
−1.004	2.839	0.634	17.633	C—C
−0.851	0.715	0.221	8.561	C—N
−0.775	2.041	0.525	13.432	N—N
−0.628	0.448	0.505	5.275	N—O
−0.153	0.983	0.481	8.087	C—H

(Bartashevich *et al.*, 2006; Tsirelson *et al.*, 2006; Howard & Lamarche, 2003), the C—N bonds are seen to have significantly lower order that the others in the five-membered rings. Although Butcher *et al.* (2003*c*) noted small differences in bond lengths in the five-membered rings, there is no obvious correlation with the properties of the bond-critical points.

We note that additional stabilization of the molecule is provided by two intramolecular closed-shell interactions – O32···O41 and O11···H6 – Table 3(*a*). The properties of the critical point on the O···O bond path are essentially identical to those previously reported for the dinitramide anion (Zhurova *et al.*, 2002).

Butcher *et al.* (2003*c*) only identify two intermolecular hydrogen bonds in (4) crystals based on distance criteria. As there may be a correlation between intermolecular interactions and impact sensitivity for energetic materials (Bader, 2006), and because we have noted close (less than van der Waals) contacts in other high-density energetic materials, *e.g.* ϵ- and γ-HNIW[4] (Bolotina *et al.*, 2004), we have carefully examined the intermolecular space for additional bond paths and characterized their (3,−1) critical points (Table 3*b*). We find 11 intermolecular interactions, four of which are hydrogen bonds, two are O···O interactions, three are O···C and two are O···N. From the properties of the critical points, these are all clearly closed-shell interactions (for example, see Fig. 6). An approximate value for the stabilization obtained from these interactions (or the energy available on their rupture) may be obtained from the potential energy density at the critical points – $D_e \simeq -v/2$ (Espinosa & Molins, 2000). Although this expression was derived for hydrogen bonds, it should also provide a reasonable estimate for other weak closed-shell interactions. Thus, summing the energies would provide 65–70 kJ mol^{-1} if all intermolecular 'bonds' were ruptured. There are few published values for these non-hydrogen-bonding weak interactions; however, from our own unpublished work (Zhurova & Pinkerton, 2007) the range of values obtained from experiment and/or calculations for 11 different energetic molecules are as follows: O···O, 1.2–21.8; O···N, 1.5–11.8; N···N, 1.6–16.9; O···C, 2.2–10.7 kJ mol^{-1}.

The atomic charge distribution has been evaluated from integration of the electron density over the atomic basins using Bader (1990) partitioning. The atomic charges thus derived from both experimental and theoretical structure factors are reported in Table 4. Therefore, the O atoms are negative, the H atoms are positive, and nitrogen bound to oxygen is positive whereas nitrogen bound to carbon is negative. All the C atoms are positive; C5, being the only carbon not bound to nitrogen, is significantly less so.

As molecule (4) is classed as an energetic material, it is of interest to determine the electronic energy distribution. The total electronic energies have been calculated and integrated over the atomic basins (Tsirelson & Stash, 2004; Zhurova *et al.*, 2002) based on the multipole-refined parameters obtained from both the experimental and theoretical structure factors. The results reported in Table 4 show that the agreement between theory and experiment is excellent. As anticipated, the regions of highest electronic energy correlate strongly with the electronegativity of the atoms.

5. Conclusion

The current study provides experimental insight into the chemical bonding in 1,3,4-trinitro-7,8-diazapentalene. In particular, conjugation in the five-membered rings is established from the topological analysis of the electron density. Asymmetry in the electrostatic potential owing to the proximity of the two nitro groups on one side of the molecule is also demonstrated. The nature of the O···H, O···O, O···N and O···C intermolecular interactions has been characterized.

We thank Dr J. C. Bottaro for providing a sample of (4), Dr E. A. Zhurova for helpful discussions, and we appreciate the financial support of the Office of Naval Research through contract number N00014-05-1-0397.

References

Allen, F. H., Kennard, O., Watson, D. G., Brammer, L., Orpen, A. G. & Taylor, R. (1987). *J. Chem. Soc. Perkin Trans. 2*, pp. S1–S19.
Bader, R. F. W. (1990). *Atoms in Molecules: A Quantum Theory*, The International Series of Monographs of Chemistry, edited by J. Halpen & M. L. H.Green. Oxford: Clarendon Press.
Bader, R. F. W. (2006). Personal communication.
Bartashevich, E. V., Potemkin, V. A., Stash, A. I. & Tsirelson, V. G. (2006). *Proc. IV National Crystal Chemistry Conference*, Chernogolovka, Russia, 26–30 June, p. 5.7.
Bergman, D. L., Laaksonen, L. & Laaksonen, A. (1997). *J. Mol. Graph. Model*, **15**, 301–306.
Bianchi, R. I., Gatti, C., Adovasio, V. & Nardelli, M. (1996). *Acta Cryst.* B**52**, 471–478.
Blessing, R. H. (1987). *Cryst. Rev.* **1**, 3–58.

[4] Hexanitrohexaazaisowurtzitane.

Blessing, R. H. (1989). *J. Appl. Cryst.* **22**, 396–397.
Bolotina, N. B., Hardie, M. J., Speer, R. L. & Pinkerton, A. A. (2004). *J. Appl. Cryst.* **37**, 808–814.
Butcher, R. J., Bottaro, J. C. & Gilardi, R. (2003*a*). *Acta Cryst.* E**59**, o1149–o1150.
Butcher, R. J., Bottaro, J. C. & Gilardi, R. (2003*b*). *Acta Cryst.* E**59**, m591–m593.
Butcher, R. J., Bottaro, J. C. & Gilardi, R. (2003*c*). *Acta Cryst.* E**59**, o1780–o1782.
Butcher, R. J., Bottaro, J. C. & Gilardi, R. (2003*d*). *Acta Cryst.* E**59**, o1777–o1779.
Coppens, P., Guru Row, T. N., Leung, P., Stevens, E. D., Becker, P. J. & Yang, Y. W. (1979). *Acta Cryst*, A**35**, 63–72.
Coppens, P. & Volkov, A. (2004). *Acta Cryst.* A**60**, 357–364.
Destro, R., Soave, R., Barzaghi, M. & Presti, L. L. (2005). *Chem. Eur. J.* **11**, 4621–4634.
Espinosa, E. & Molins, E. (2000). *J. Chem. Phys.* **11**, 5686–5694.
Flaig, R., Koritsanszky, T., Dittrich, B., Wagner, A. & Luger, P. (2002). *J. Am. Chem. Soc.* **124**, 3407–3417.
Frisch, M. J. *et al.* (1998). *GAUSSIAN.* Gaussian Inc., Pittsburgh PA, USA.
Hansen, N. & Coppens, P. (1978). *Acta Cryst.* A**34**, 909–921.
Henn, J., Ilge, D., Leusser, D., Stalke, D. & Engels, B. (2004). *J. Phys. Chem. A*, **108**, 9442–9452.
Hirshfeld, F. L. (1976). *Acta Cryst.* A**32**, 239–244.
Howard, S. T. & Lamarche, O. (2003). *J. Phys. Org. Chem.* **16**, 133–141.
Koritsanszky, T., Richter, T., Macchi, P., Gatti, C., Howard, S., Mallinson, P. R., Farrugia, L., Su, Z. W. & Hansen, N. K. (2003). *XD*. Technical Report, Freie Universität Berlin, Berlin, Germany.
Laaksonen, L. (1992). *J. Mol. Graph.* **10**, 33–34.
Murray, J. S., Lane, P. & Politzer, P. (1995). *Mol. Phys.* **85**, 1–8.
Rice, B. M. & Hare, J. J. (2002). *J. Phys. Chem. A*, **106**, 1770–1783.
Ritchie, J. P., Zhurova, E. A., Martin, A. & Pinkerton, A. A. (2003). *J. Phys. Chem. B*, **107**, 14576–14589.
Saunders, V. R., Dovesi, R., Roetti, C., Causà, M., Harrison, N. M., Orlando, R. & Sicovich-Wilson, C. M. (1998). *CRYSTAL98 User's Manual.* University of Torino, Italy.
Sheldrick, G. M. (1997). *SHELXTL*, Version 5.1. University of Göttingen, Germany.
Siemens (1996). *SAINT.* Siemens Analytical X-ray Instruments Inc., Madison, Wisconsin, USA.
Smith, G. T., Mallinson, P. R., Frampton, C. S. & Howard, J. A. K. (1997). *J. Chem. Soc. Perkin Trans. 2*, pp. 1329–1333.
Spackman, M. A., Byrom, P. G., Alfredsson, M. & Hermansson, K. (1999). *Acta Cryst.* A**55**, 30–47.
Stash, A. I. & Tsirelson, V. G. (2002). *J. Appl. Cryst.* **35**, 371–373.
Stash, A. I. & Tsirelson, V. G. (2005). *Crystallogr. Rep.* **50**, 202–209.
Su, Z. & Coppens, P. (1992). *Acta Cryst.* A**48**, 188–187.
Tsirelson, V. G. & Ozerov, R. P. (1996). *Electron Density and Bonding in Crystals*, pp. 1–517. London: Institute Of Physics Publishing.
Tsirelson, V. G., Ivanov, Yu., Zhurova, E. A., Zhurov, V. V. & Tanaka, K. (2000). *Acta Cryst.* B**56**, 197–203.
Tsirelson, V. G. & Stash, A. I. (2004). *Acta Cryst.* A**60**, 418–426.
Tsirelson, V. G., Stash, A. I., Potemkin, V. A., Rykounov, A. A., Shutalev, A. D., Zhurova, E. A., Zhurov, V. V., Pinkerton, A. A., Gurskaya, G. V. & Zavodnik, V. E. (2006). *Acta Cryst.* B**62**, 676–688.
Volkov, A., Abramov, Yu., Coppens, P. & Gatti, C. (2000). *Acta Cryst.* A**56**, 332–339.
Volkov, A., Koritsanszky, T., Li, X. & Coppens, P. (2004). *Acta Cryst.* A**60**, 638–639.
Wu, G., Rodrigues, B. L. & Coppens, P. (2002). *J. Appl. Cryst.* **35**, 356–359.
Zhurova, E. A., Martin, A. & Pinkerton, A. A. (2002). *J. Am. Chem. Soc.* **124**, 8741–8750.
Zhurova, E. A. & Pinkerton, A. A. (2001). *Acta Cryst.* B**57**, 359–365.
Zhurova, E. A. & Pinkerton, A. A. (2007). To be published.
Zhurova, E. A., Tsirelson, V. G., Stash, A. I. & Pinkerton, A. A. (2002). *J. Am. Chem. Soc.* **124**, 4574–4575.
Zhurova, E. A., Stash, A. I., Tsirelson, V. G., Zhurov, V. V., Bartashevich, E. V., Potemkin, V. A. & Pinkerton, A. A. (2006). *J. Am. Chem. Soc.* **128**, 14728–14734.
Zhurova, E. A., Tsirelson, V. G., Stash, A. I., Yakoulev, M. V. & Pinkerton, A. A. (2004). *J. Phys. Chem. B*, **108**, 20173–20179.